Chemistry of Metals and Alloys

Chem. Met. Alloys 13 (2020) 70-77
Ivan Franko National University of Lviv
www.chemetal-journal.org

$Y_{1-x}Dy_xSn_{2-y}M_y$ (M = Sb, Pb) electrode materials activated by CNT and Mg–T–Ga (T = Co, Ni) phases for lithium- and sodium-ion batteries

Volodymyr PAVLYUK[1,2]*, Wojciech CIESIELSKI[2], Nazar PAVLYUK[1], Hryhoriy DMYTRIV[1], Damian KULAWIK[2], Agnieszka BALIŃSKA[2], Karolina KLUZIAK[2]

[1] *Department of Inorganic Chemistry, Ivan Franko National University of Lviv, Kyryla i Mefodiya St. 6, 79005 Lviv, Ukraine*
[2] *Institute of Chemistry, Jan Długosz University of Częstochowa, Al. Armii Krajowej 13/15, 42-200 Częstochowa, Poland*
* *Corresponding author. E-mail: vpavlyuk2002@yahoo.com*

Received October 20, 2020; accepted December 29, 2020; available on-line January 4, 2021
https://doi.org/10.30970/cma13.0408

The new quaternary $Y_{1-x}Dy_xSn_{2-y}M_y$ (M = Sb, Pb) phases crystallize as maximally disordered (MD) representatives with the orthorhombic structure type $ZrSi_2$. During electrochemical lithiation and sodiation, the formation of $Y_{1-x}Dy_xSn_{2-y}M_yLi_z$ and $Y_{1-x}Dy_xSn_{2-y}M_yNa_z$ maximally disordered – high-entropy intermetallic phases (MD-HEIP), as the result of insertion of Li/Na into structural voids, was observed. Carbon nanotubes (CNT) and Mg–T–Ga (T = Co, Ni) phases are efficient catalytic additives to improve the cycling stability of the anodes for lithium-ion (LIBs) and sodium-ion batteries (SIBs). The results show that the catalysts can increase the electrode capacities up to 15 % for LIBs and up to 10 % for SIBs.

Intermetallic compound / Crystal structure / Lithium-ion battery/ Sodium-ion battery

Introduction

Multicomponent intermetallics with sufficiently large voids are favorable for the insertion of Li^+ or Na^+ ions. The insertion of lithium atoms into octahedral voids of hexagonal Zr_5Sn_3 and RE_5M_3 (RE = Y, La, Gd; M = Ge, Sn) binary phases was described in [1-3]. The crystal structures of the RE_5M_3 intermetallic compounds belong to the Mn_5Si_3-type. For this binary structure, the presence of an octahedral void in Wyckoff position 2*b* is typical. The incorporation of a third element (alkaline or transition metal, T) into the 2*b* site leads to the formation of a RE_5TM_3 ternary phase with a Hf_5CuSn_3-type structure [4]. Two mechanisms of *substitution* and *insertion* for the modification of the binary $GdSn_2$ structure ($ZrSi_2$-type) have been proposed [5]. By the first mechanism, due to partial replacement of Gd by La and Sn by Sb atoms, a four-component maximally disordered (MD) phase of composition $Gd_{1-x}La_xSn_{2-y}Sb_y$ was obtained. By the second mechanism, due to insertion of Li or Mg atoms into tetragonal antiprism, maximally disordered – high-entropy intermetallic phases (MD-HEIP) $Gd_{1-x}La_xSn_{2-y}Sb_yM_z$ (M = Li, Na, Mg) were prepared [5].

Additives in the form of carbon nanotubes (CNT) and transition-metal oxides (TMOs) improved the charge transfer process and activated the surface area of the electrodes, which results in excellent electrochemical lithium/charge storage properties when evaluated as electrode materials for lithium-ion batteries and electrochemical capacitors [6].

In this paper, we present results obtained on the structural and electrochemical (lithiation and sodiation) properties of $Y_{1-x}Dy_xSn_{2-y}M_y$ (M = Sb, Pb) phases by modification with CNT and Mg–T–Ga (T = Co, Ni) composites.

Experimental section

Elements with a nominal purity of more than 99.9 wt.% were used as starting components for preparing alloys by arc-melting of stoichiometric amounts of the pure metals in an argon atmosphere. The ingots were homogenized in quartz ampoules under vacuum at 670 K for 300 h.

After melting and annealing, the total weight loss was less than 2 %. Small good-quality single crystals of the $Y_{1-x}Dy_xSn_{2-y}M_y$ (*M* = Sb, Pb) phases were isolated from the alloys.

Single-crystal data were collected at room temperature by using a four-circle diffractometer (*Xcalibur Oxford Diffraction*) with a CCD detector (graphite monochromatized Mo *K*α radiation, λ = 0.071073 nm). Scans were performed in the ω mode, empirical absorption corrections were made by CrysAlis RED [7]. The crystal structures of the quaternary compounds investigated in the present work were successfully solved by direct methods and refined using SHELX-97 package programs [8].

The alloys were studied by wavelength-dispersive spectrometry (WDS) and electron probe microanalysis (EPMA), using a TESCAN scanning electron microscope (SEM).

A potentiostat–galvanostat from CH Instruments (Austin, TX, USA) was used to measure all electrochemical relationships. The electrode materials were prepared by grinding powders containing 80 wt.% $Y_{1-x}Dy_xSn_{2-y}M_y$ (active material), 10 wt.% black carbon (electronically conductive additive), and 10 wt.% polyvinylidene fluoride (PVDF binder) in an agate mortar. The mixtures were pressed onto a stainless-steel grid (about 5 mg, diameter 11 mm). The $Y_{1-x}Dy_xSn_{2-y}M_y$ electrodes were modified by composite additives (CA), which consisted of carbon nanotubes (CNT) and Mg–*T*–Ga (*T* = Co, Ni) phases. The modified electrodes were prepared from powdered $Y_{1-x}Dy_xSn_{2-y}M_y$ (85 wt.%), Mg–*T*–Ga (5 wt.%), CNT (5 wt.%) and 5 wt.% polyvinylidene fluoride (PVDF binder). The components were mixed, pressed into pellets and sintered at a temperature of 400°C for 10 h.

The charge-discharge curves were performed in two-electrode Swagelok-type cells (coin prototype). The lithium cells contained an $Y_{1-x}Dy_xSn_{2-y}M_y$ electrode as a working electrode with Li reference and $LiCoO_2$ counter electrodes and the sodium cells contained Na as a reference and Na_xCoO_2 as a counter electrode. Electrochemical impedance spectroscopy (EIS) of the alloys was performed in three-electrode cells with $Y_{1-x}Dy_xSn_{2-y}M_y/LiCoO_2$ electrodes (in the case lithium-ion cells) or $Y_{1-x}Dy_xSn_{2-y}M_y/Na_xCoO_2$ (in the case of sodium-ion cells). Ethylencarbonate/ dimethylcarbonate nonaqueous electrolytes containing Li^+ or Na^+ ions were used. The anode and cathode sections were separated by an electrolyte-impregnated Celgard 2320 separator.

Results and discussion

The binary compound YSn_2 was modified to a maximally disordered – high-entropy intermetallic phase (MD-HEIP) with general formula $Y_{1-x}Dy_xSn_{2-y}M_yL_z$ (where *M* = Sb or Pb; *L* = Li or Na) by *substitution* and *insertion* steps. For the partial substitution of the Y atoms in Wyckoff position 4*c*, Dy was used, and Sb or Pb was used for the partial substitution of Sn atoms. As a result of this substitution, maximum disordered (MD) phases of $Y_{1-x}Dy_xSn_{2-y}M_y$ are formed. In the structure of the binary phase $GdSn_2$, there are empty tetragonal antiprisms, into which lithium or sodium can be inserted. According to the literature [9,10], insertion of lithium into the antiprisms of RSn_2 (*R* = rare-earth metal) phases leads to the formation of an ordered $RLiSn_2$ phase, which belongs to the structure type $CeNiSi_2$, which is derived from the $ZrSi_2$-type. If Li or Na atoms, or others, are introduced into the voids of the maximally disordered (MD) phase, a high-entropy intermetallic phase (HEIP) is formed, which contains five elements whose contents exceed 5 at.%.

Since $Y_{1-x}Dy_xSn_{2-y}M_y$ is a multicomponent compound, it was important to use single-crystal diffraction to accurately determine the distribution of the atoms on the crystallographic sites. The general structural results are summarized in Table 1. Detailed structural refinements showed that only lithium can be inserted into the tetragonal antiprisms, whereas sodium is not inserted but partially replaces tin atoms, forming a split site with them. The refined atomic coordinates and displacement parameters for the investigated $Y_{1-x}Dy_xSn_{2-y}M_y$ single crystals are presented in Table 2.

According to the X-ray diffraction (Fig. 1) and electron microscopic (Fig. 2) examinations, the $Y_{1-x}Dy_xSn_{2-y}M_y$ (*M* = Sb, Pb) compounds before lithiation and sodiation contain only the $ZrSi_2$-type phase. Electrochemical lithiation/sodiation at a low current density (0.1 mA cm^{-2}) was conducted for an accurate and detailed determination of the electrochemical reaction of $Y_{1-x}Dy_xSn_{2-y}M_y$ (*M* = Sb, Pb) with lithium and sodium at room temperature. As show only the orthorhombic phase with $ZrSi_2$-type, and the shift of the diffraction peaks reflects the expansion of the crystal lattice during the lithiation process. However, the pattern of the sample corresponding to the second plateau with a maximum value of $z > 1.0$ contains two phases. According to phase analysis, at $z = 1.2$ in addition to residues of the orthorhombic phases a new phase $Li_m(Sn/Sb)_k$ is observed (Fig. 3a). Thus, the total lithiation process occurs in two stages. The first one is the insertion of lithium into structural voids, and the second one is the decomposition of the orthorhombic phase into new phases and replacement of tin atoms by lithium. This process is reversible, so we can introduce the general scheme of lithiation/delithiation:

$$\text{I. } (Y/Dy)(Sn/Sb)_2 + zLi^+ + ze^- \underset{}{\overset{\text{insertion}}{\rightleftharpoons}} (Y/Dy)(Sn/Sb)_2Li_z$$

$$\text{II. } (Y/Dy)(Sn/Sb)_2Li_z + (k+m)Li^+ + (k+m)e^- \underset{\text{decomposition /substitution}}{\overset{}{\rightleftharpoons}} (Y/Dy)(Sn/Sb)_{2-k}Li_{z+k} + Li_m(Sn/Sb)_k$$

Table 1 Crystal data and structure refinement.

Empirical formula	$Y_{1-x}Dy_xSn_{2-y}Sb_y$	$Y_{1-x}Dy_xSn_{2-y}Pb_y$
Formula weight	343.98 g mol^{-1}	343.96 g mol^{-1}
Temperature	293 K	293 K
Wavelength	Mo *Kα*, 0.71073 Å	Mo *Kα*, 0.71073 Å
Crystal system, space group	orthorhombic, *Cmcm* (63)	orthorhombic, *Cmcm* (63)
Unit-cell dimensions	*a* = 4.4008(6) Å	*a* = 4.4409(6) Å
	b = 16.427(1) Å	*b* = 16.4674(10) Å
	c = 4.3727(5) Å	*c* = 4.3927(5) Å
Volume	316.13(6) Å^3	321.24(6) Å^3
Calculated density	8.558 g cm^{-3}	8.614 g cm^{-3}
Absorption coefficient	17.43 mm^{-1}	17.15 mm^{-1}
F(000)	581	580
Theta range for data collection	θ_{max} = 26.4°, θ_{min} = 4.8°	θ_{max} = 26.3°, θ_{min} = 4.8°
Index ranges	$-5 \le h \le 5$, $-20 \le k \le 20$,	$-4 \le h \le 5$, $-20 \le k \le 16$,
	$-5 \le l \le 5$	$-5 \le l \le 4$
Reflections collected/unique	1100/208	1042/211
Refinement method	Refinement on F^2	Refinement on F^2
	Least-squares matrix: full	Least-squares matrix: full
Data/parameters	208/15	229/18
Goodness of fit on F^2	1.19	1.20
$R[F^2 > 2\sigma(F^2)]$	0.033	0.053
$wR(F^2)$	0.096	0.134
Extinction coefficient	0.0014(4)	0.0013(6)
Largest difference peak and hole	3.49 and -2.46 e Å^{-3}	4.09 and -2.49 e Å^{-3}

Table 2 Fractional atomic coordinates and displacement parameters for $Y_{1-x}Dy_xSn_{2-y}Sb_y$ and $Y_{1-x}Dy_xSn_{2-y}Pb_y$ (Å^2).

Atom	**Site**	***x*/*a***	***y*/*b***	***z*/*c***	U_{eq}	**Occ.**
			$Y_{1-x}Dy_xSn_{2-y}Sb_y$			
Y1	4*c*	0	0.40085(6)	¼	0.0039(5)	0.60
Dy1	4*c*	0	0.40085(6)	¼	0.0039(5)	0.40
Sn1	4*c*	0	0.75136(10)	¼	0.0131(6)	0.80
Sb1	4*c*	0	0.75136(10)	¼	0.0131(6)	0.20
Sn2	4*c*	0	0.06227(10)	¼	0.0122(6)	1.00
	U^{11}	U^{22}	U^{33}	U^{12}	U^{13}	U^{23}
Y1	0.0051(7)	0.0046(7)	0.0021(7)	0	0	0
Dy1	0.0051(7)	0.0046(7)	0.0021(7)	0	0	0
Sn1	0.0128(9)	0.0136(9)	0.0129(9)	0	0	0
Sb1	0.0128(9)	0.0136(9)	0.0129(9)	0	0	0
Sn2	0.0087(8)	0.0194(9)	0.0086(8)	0	0	0
			$Y_{1-x}Dy_xSn_{2-y}Pb_y$			
Y1	4*c*	0	0.40098(11)	¼	0.0015(9)	0.60
Dy1	4*c*	0	0.40098(11)	¼	0.0015(9)	0.40
Sn1	4*c*	0	0.75141(17)	¼	0.0152(10)	0.90
Pb1	4*c*	0	0.75141(17)	¼	0.0152(10)	0.10
Sn2	4*c*	0	0.06271(18)	¼	0.0146(10)	1.00
	U^{11}	U^{22}	U^{33}	U^{12}	U^{13}	U^{23}
Y1	0.0012(12)	0.0034(12)	0.0000(11)	0	0	0
Dy1	0.0012(12)	0.0034(12)	0.0000(11)	0	0	0
Sn1	0.0153(16)	0.0167(16)	0.0137(16)	0	0	0
Y1	0.0012(12)	0.0034(12)	0.0000(11)	0	0	0
Dy1	0.0012(12)	0.0034(12)	0.0000(11)	0	0	0

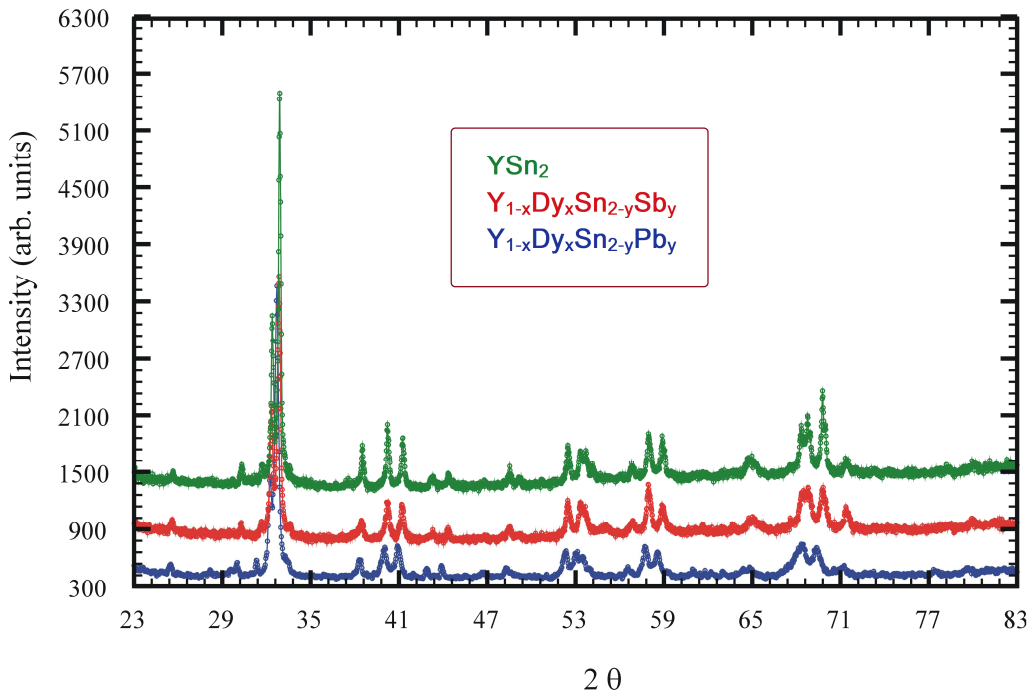

Fig. 1 X-ray powder diffraction pattern for YSn_2, $Y_{1-x}Dy_xSn_{2-y}Sb_y$ and $Y_{1-x}Dy_xSn_{2-y}Pb_y$.

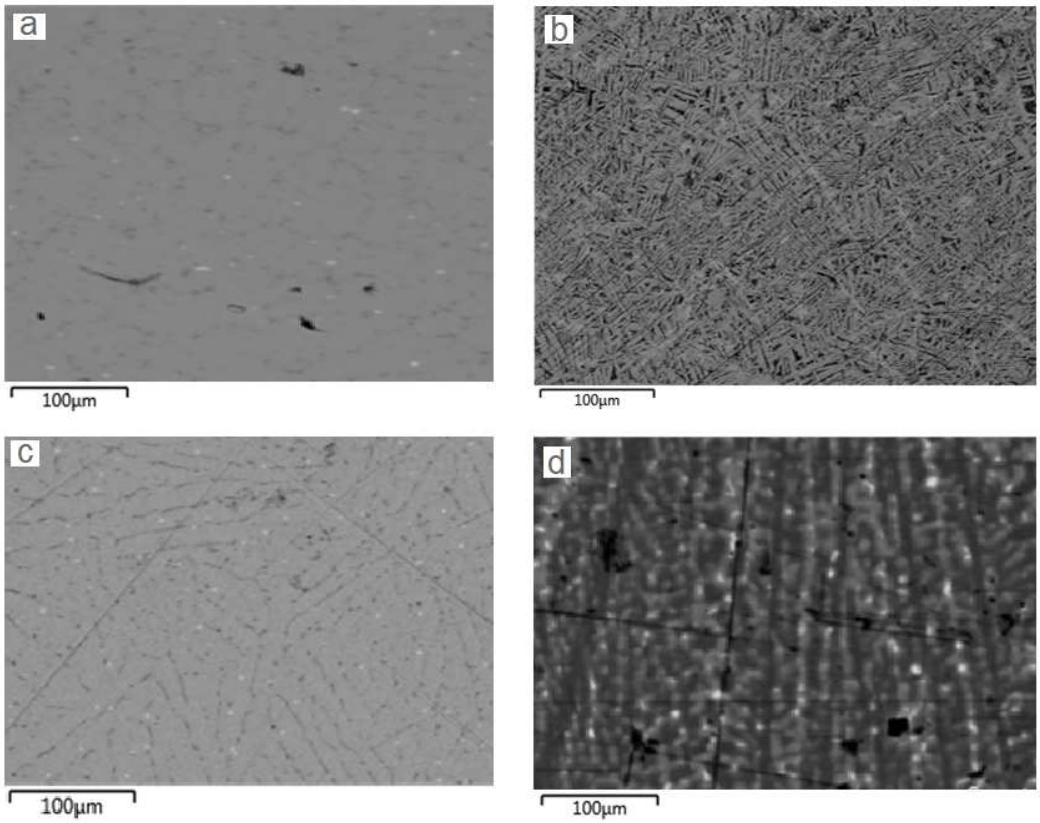

Fig. 2 Scanning electron microscopy images for initial and modified samples: $Y_{1-x}Dy_xSn_{2-y}Sb_y$ (a), $Y_{1-x}Dy_xSn_{2-y}Sb_y$–CA (b), $Y_{1-x}Dy_xSn_{2-y}Pb_y$ (c) and $Y_{1-x}Dy_xSn_{2-y}Pb_y$–CA (d).

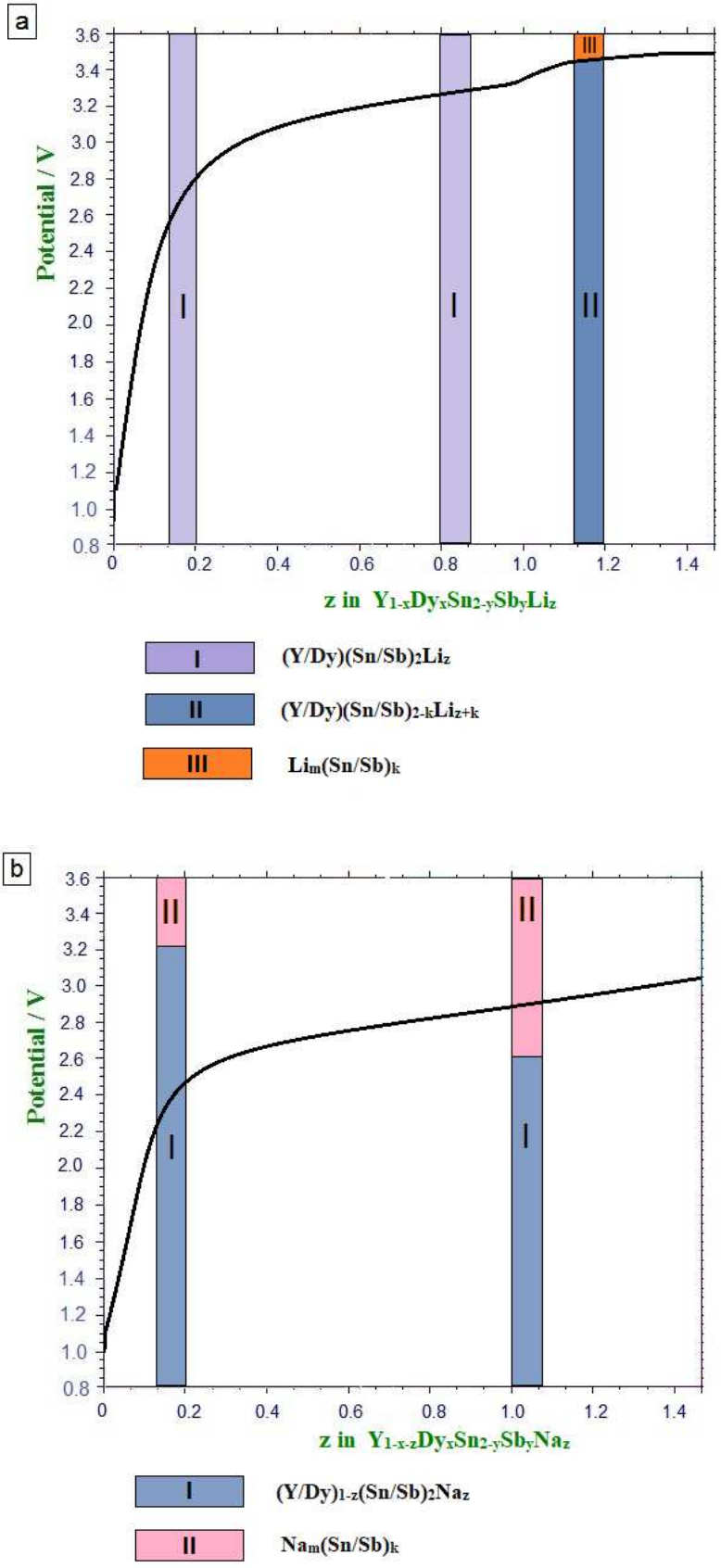

Fig. 3 First-charge curves and phase contents for the electrodes $Y_{1-x}Dy_xSn_{2-y}Sb_yLi_z$ (a) and $Y_{1-x}Dy_xSn_{2-y}Pb_yNa_z$ (b).

For the sodiation process, only one plateau is observed for (Y/Dy)(Sn/Sb)$_2$ (Fig. 3b), which corresponds to the electrochemical substitution by sodium of constituent elements in the orthorhombic phase ($ZrSi_2$-type). The electrochemical sodiation/desodiation process (Fig. 3b) occurs in one stage:

$$(Y/Dy)(Sn/Sb)_2 + zNa^+ + ze^- \underset{}{\overset{insertion}{\rightleftharpoons}} (Y/Dy)_{1-z}(Sn/Sb)_{2-k}Na_z + (Y/Dy)_z(Sn/Sb)_k$$

Discharge curves for the tested $Y_{1-x}Dy_xSn_{2-y}M_y$ (*M* = Sb, Pb) electrodes are shown in Figs. 4a,b. For the discharge processes, from 3.3 V to 1.8 V for Li-ion cells and from 3.0 V to 1.5 V for Na-ion cells, better discharge characteristics were observed for electrodes doped with composite additives (CA). The effect of the addition of carbon nanotubes (CNT) and Mg–*T*–Ga (*T* = Co, Ni) phases on the improvement of the hydrogen sorption kinetics of the intermetallic phase is due to the following factors:

- CNT improve the electrical connectivity within the electrode, thus improving the capacity by connecting and maintaining more electron conduction pathways between the active material and the current collector;
- Mg–*T*–Ga additives, by filling the intergranular space during sintering, activate the grain surface of the $Y_{1-x}Dy_xSn_{2-y}M_y$ alloy, causing a decrease of the activation energy for the insertion/deinsertion of lithium or sodium ions during the charge/discharge processes.

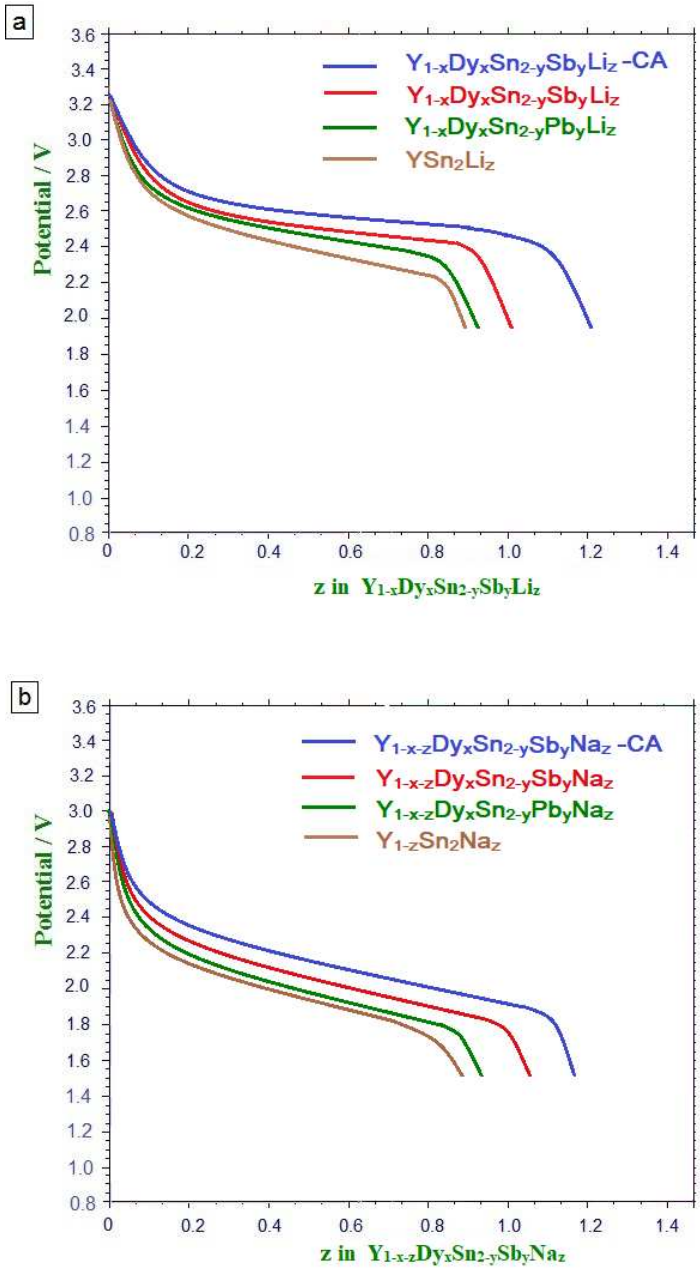

Fig. 4 Discharge potential curves of electrodes for Li-ion cells (a) and Na-ion cells (b).

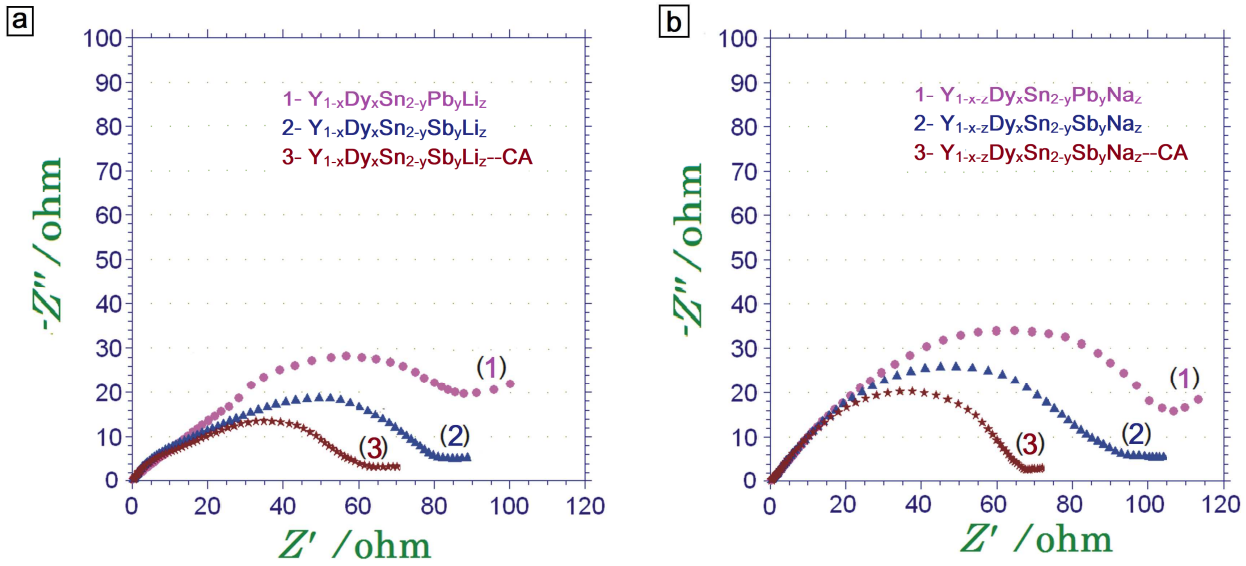

Fig. 5 Electrochemical impedance spectra (EIS) of the electrodes for Li-ion cells (a) and Na-ion cells (b).

As additives to the electrodes, Laves phases $MgT_{2-x}Ga_x$, $MgCoGa_2$, $MgCo_2Ga_5$, $MgNi_2Ga_5$, $Mg_9Ni_6Ga_{14}$ and Mg_3Ni_2Ga from Mg–*T*–Ga ternary system [11-13] were used.

Electrochemical impedance spectroscopy (EIS) is an important electrochemical method for investigating the kinetics of the electrode and the reactions taking place on its surface, and has been successfully used in the study of Li- and Na-ion electrodes. Fig. 5 shows the EIS curves of the initial and modified $Y_{1-x}Dy_xSn_{2-y}M_y$ (*M* = Sb, Pb) electrodes after the first charge/discharge cycles (charging at 5 mA for 1800 s and discharging at 1 mA to −1.5 V). It can be seen from Fig. 5a (for Li-ion cells) and Fig. 5b (for Na-ion cells), that the diameter of the semicircle in the high-frequency region decreases in the sense $Y_{1-x}Dy_xSn_{2-y}Pb_y \rightarrow Y_{1-x}Dy_xSn_{2-y}Sb_y \rightarrow Y_{1-x}Dy_xSn_{2-y}Sb_y$–CA. This means that substitution followed by CA-modification increases the charge-transfer capability on the electrode surface.

Moreover, as shown in Fig. 5, the diameters of the semicircles of the CA-modified electrodes are smaller than those of the $Y_{1-x}Dy_xSn_{2-y}Sb_y$ and $Y_{1-x}Dy_xSn_{2-y}Pb_y$ electrodes, which demonstrates that the charge-transfer reaction is facilitated for the $Y_{1-x}Dy_xSn_{2-y}Sb_y$–CA electrodes. This also indicates that CA-modification improves the catalytic activity of the electrode surface.

Acknowledgements

Financial support from the National Science Center, Poland (No. 2017/25/B/ST8/02179) is gratefully acknowledged.

References

[1] A. Balinska, V. Kordan, R. Misztal, V. Pavlyuk, *J. Solid State Electrochem.* 19 (2015) 2481-2490.
[2] V. Pavlyuk, A. Stetskiv, B. Rozdzynska-Kielbik, *Intermetallics* 43 (2013) 29-37.
[3] A. Stetskiv, V. Kordan, I. Tarasiuk, O. Zelinska, V. Pavlyuk, *Chem. Met. Alloys* 7 (2014) 106-111.
[4] V. Pavlyuk, A.Balinska , B. Rozdzynska-Kiełbik, N. Pavlyuk , G. Dmytriv, A. Stetskiv, S. Indris, B. Schwarz, H. Ehrenberg, *J. Alloys Compd*. 838 (2020) 155643.
[5] H. Zhou, L. Zhang, D. Zhang, *Sci. Rep*. 6 (2016) 37752.
[6] V. Yao, C.Z. Wu, H. Wang, H.M. Cheng, G.Q. Lu, *J. Nanosci. Nanotechnol.* 6 (2006) 494-498.
[7] CrysAlis RED, Version 1.171, Oxford Diffraction Ltd, Abingdon, UK, 2005.
[8] G.M. Sheldrick, SHELXL-97: Program for Crystal Structure Refinement, University of Goettingen, Germany, 1997.
[9] V.V. Pavlyuk, O.I. Bodak, V.K. Pecharskii, R.V. Skolozdra, E.I. Gladyshevskii, *Inorg. Mater*. 25 (1989) 1145-1148.
[10] J.P.A. Makongo, N.-T. Suen, S. Guo, *J. Solid State Chem*. 211 (2014) 95-105.
[11] N. Pavlyuk, G. Dmytriv, V. Pavlyuk, B. Rozdzynska-Kielbik, W. Nitek, W. Lasocha, I. Chumak, H. Ehrenberg, *Acta Cryst. C* 76(6) (2020) 541-546.

[12] N. Pavlyuk, G. Dmytriv, V. Pavlyuk, B. Rozdzynska-Kielbik, A. Gil, I. Chumak, H. Ehrenberg, *Z. Kristallogr*. 235(11) (2020) 513-521.

[13] N. Pavlyuk, G. Dmytriv, V. Pavlyuk, B. Rozdzynska-Kielbik, G. Cichowicz, M.K. Cyranski, I. Chumak, H. Ehrenberg. *Acta Cryst. B* 76(4) (2020) 534-542.